JOURNAL OF GEOPHYSICAL RESEARCH, VOL. 105, NO. C1, PAGES 1037–1053, JANUARY 15, 2000

Upper equatorial Pacific Ocean current and salinity variability during the 1996–1998 El Niño–La Niña cycle

Gregory C. Johnson and Michael J. McPhaden

NOAA Pacific Marine Environmental Laboratory, Seattle, Washington

G. Dail Rowe

Department of Oceanography, University of Hawaii, Honolulu

Kristene E. McTaggart

NOAA Pacific Marine Environmental Laboratory, Seattle, Washington

Abstract. The recent El Niño–La Niña cycle exhibited striking patterns of current and salinity variability in the upper equatorial Pacific Ocean. This evolution is described from mid-1996 through 1998 using a remarkable data set of 35 meridional conductivity-temperature-depth (CTD)/acoustic Doppler current profiler (ADCP) sections along with buoy data. The sections, nominally from 8°S to 8°N between 165°E and 95°W, were occupied over the course of 27 months. A wide range of current variability was sampled with currents that appeared or disappeared some time during the cycle, including an equatorially trapped eastward surface current, the Equatorial Undercurrent, the northern branch of the South Equatorial Current, and the North Equatorial Countercurrent. Basin-wide, interannual changes in upper ocean and pycnocline zonal transports were as large as $64 \pm 32 \times 10^6$ m^3 s^{-1}. Changes in the salinity structure included a deep and fresh mixed layer in the central equatorial Pacific that built up during the El Niño and was then disrupted by upwelled salty water with the onset of La Niña, a very fresh mixed layer observed in the eastern equatorial Pacific late in the El Niño, and a reduction in the strength of the meridional equatorial salinity gradient within the pycnocline to one third of the usual value during the El Niño. Finally, the zonal transports above the thermocline from 5°S to 5°N were well correlated with the rate of change of warm-water volume west of the individual CTD/ADCP sections.

1. Introduction

The 1997–1998 El Niño was by many measures the strongest on record. Because of the presence of the El Niño-Southern Oscillation (ENSO) Observing System [*McPhaden et al.*, 1998], this El Niño and the subsequent La Niña were also the best sampled ENSO events. A major component of the ENSO Observing System is the Pacific Ocean Tropical Atmosphere-Ocean (TAO) moored buoy array, data from which have been used to describe the onset and rapid decay of this El Niño [*McPhaden*, 1999]. Here we study upper ocean current and salinity changes across the tropical Pacific associated with the recent El Niño–La Niña cycle, primarily using 35 conductivity-temperature-depth (CTD) and shipboard acoustic Doppler current profiler (ADCP) sections routinely occupied from September 1996 through November 1998 from 8°S to 8°N between 165°E and 95°W during TAO mooring cruises.

Studies of upper equatorial Pacific Ocean current and water mass variability during previous Los Niños have been regionally focused. Most studies of the 1982–1983 El Niño current and water mass variability using shipboard ADCP and CTD data are limited to the central [*Firing et al.*, 1983] and the eastern [*Toole and Borges*, 1984; *Mangum et al.*, 1986; *Hayes et al.*, 1987] Pacific. Similar studies for the 1986–1988 El Niño-La Niña cycle are limited to the eastern [*McPhaden and Hayes*, 1990] and western [*Delcroix et al.*, 1992] Pacific. Similar work on the effects of westerly wind bursts in 1989–1990 focused on the western and central Pacific [*McPhaden et al.*, 1992; *Kuroda and McPhaden*, 1993]. Analyses of moored data for previous events were also often geographically limited, for instance, in the eastern Pacific

Copyright 2000 by the American Geophysical Union.

Paper number 1999JC900280.
0148-0227/00/1999JC900280$09.00

for the 1982–1983 El Niño [*Halpern,* 1987], in the western Pacific for the 1986–1987 El Niño [*McPhaden et al.,* 1990], and in the central Pacific for the 1991–1993 El Niño [*Kessler and McPhaden,* 1995].

The extensive temporal and spatial coverage of the data used here allows a basin-wide study that is organized as follows. The ADCP and CTD data processing and gridding are documented first. The temporal evolution of zonal velocity and salinity are then described using vertical meridional sections. TAO buoy data give the section data a temporal context. Next, zonal volume fluxes in two layers bounded by potential isopycnals are presented. After this, upper ocean zonal volume fluxes are compared with warm-water volume budgets derived from TAO buoy data. The paper concludes by relating the 1997–1998 El Niño to previous ones.

2. Data

Servicing of the TAO moorings by the National Oceanic and Atmospheric Administration (NOAA) ship *Ka'imimoana* (and occasionally the NOAA ship *Ronald H. Brown*) affords regular occupation of equatorial Pacific Ocean CTD/ADCP sections. Longitude 165°E is visited once a year, while 180°, 170°W, 155°W, 140°W, 125°W, 110°W, and 95°W are visited twice a year. CTD stations are nominally taken to 1000 dbar at 1° latitude intervals from 8°S to 8°N, except at 140°W, where the nominal latitude range is from 5°S to 9°N. Station spacing and latitudinal extent vary in practice. Shipboard ADCP data are collected continuously, starting near 25 m and extending as deep as 450 m.

The ADCP data processing details were as described by *Firing* [1992], with the proviso that Ashtech 3DF global positioning system heading information [*King and Cooper,* 1993] was generally available. The NOAA ship *Ka'imimoana* was originally equipped with an RD Instruments (RDI) 150 khz broadband ADCP, but an RDI 150 khz narrowband ADCP (with which the *Ronald H. Brown* was also equipped) was installed in early 1997. The only relevant difference here is that the narrowband instrument has significantly more depth range than the broadband; hence ADCP sections from 1996 cruises did not extend as deep as later sections (Plate 1). ADCP data were typically reduced to 8 m vertical and 300 s temporal resolution, which yields 1.8 km along-track spatial resolution at a cruising speed of 6 m s^{-1}. Errors in the ADCP velocity measurements were generally <0.05 m s^{-1}, small compared to the large variability described here.

All ADCP data were regridded to integer multiples of 10 m in the vertical and 0.1° in latitude. The CTD profiles were used to correct ADCP depths for the difference between nominal and true sound speed. The zonal velocity data were then objectively mapped [*Bretherton et al.,* 1976] to 10 m vertical and 0.2° latitude meridional resolution. For the maps a Gaussian covariance with correlation lengths of 20 m in the vertical and 1° latitude in the meridional was used with an error-to-signal energy of 0.01. The map means were determined locally as a planar fit weighted using the correlation lengths and covariance function. The length scales were estimated from the spatial autocorrelations of the zonal velocity data, and the error energy was derived from an estimate of order 0.1 m s^{-1} noise from instrumental uncertainties, internal waves, and tides superimposed on the order of 1.0 m s^{-1} signal of the large-scale currents and planetary waves.

The CTD data were taken with Sea-Bird Electronics Incorporated 911plus CTDs equipped with dual conductivity and temperature sensors. Data calibration and processing are documented elsewhere [*McTaggart et al.,* 1997; *McTaggart and Johnson,* 1999], so only a short summary is given here. Temperature and pressure accuracies are 0.002°C and 1 dbar, respectively. Water samples were typically collected at 12 selected pressures during each cast. These samples were analyzed on board for salinity using a Guildline Model 8400B inductive salinometer standardized with International Association for Physical Sciences of the Oceans (IAPSO) standard seawater. CTD salinities, calibrated using these water sample data, are accurate to 0.003 or better. (Since salinity is determined as a ratio by the 1978 practical salinity scale (PSS-78), it is only proper to cite it without units.) Casts extended from the surface to at least 1000 dbar. Final data were processed to 1 dbar vertical resolution.

The nominal 1° latitude CTD station spacing precluded objectively mapping the CTD data in the same manner as the ADCP data. To put the CTD data on the same grid as the ADCP data while interpolating in potential density coordinates, the following procedures were implemented. Profiles of salinity S, potential temperature θ, and potential density σ_θ from each station were smoothed with a 10 dbar half-width Hanning filter. The mean mixed layer S, θ, and pressure P for each station were determined using a $\sigma_\theta = 0.05$ kg m^{-3} increase from the surface value for the mixed layer criterion. The vertical axis of each station was transformed from a regular P grid to a regular σ_θ grid. The mixed layer Ps and σ_θ grid Ps were linearly interpolated in latitude to the midpoints between stations for well-behaved splining. The combined P values were splined to 0.2° latitude meridional resolution. The station θs and Ss of the mixed layer and σ_θ grid were linearly interpolated to 0.2° latitude meridional resolution. The vertical axis for these Ss and θs was transformed back to a regular P grid. Mixed layer values of S and θ were substituted in this P grid where appropriate. Temperature and σ_θ were recalculated to remove small inconsistencies due to the series of manipulations. Finally, the vertical axis was transformed from a P grid to a 10-m resolution depth grid to match the vertical distribution of the mapped ADCP data.

Equatorial 20°C isotherm depths and zonal winds from the TAO buoys place the temporally sparse sec-

tion data in context. The 20°C isotherm is a proxy for the equatorial Pacific pycnocline [*Kessler,* 1990]. On the equator, 20°C corresponds to $\sigma_\theta = 24.87 \pm 0.12$ kg m^{-3} (± 0.26 kg m^{-3} between 5°S and 5°N), only slightly denser than the regional pycnocline core of $\sigma_\theta = 24.25$ kg m^{-3}. The standard deviations are due to regional variations in the mean temperature-salinity relation. Similarly derived root-mean-square pressure differences between the 20°C isotherm and $\sigma_\theta = 24.87$ kg m^{-3} are ± 4 dbar on the equator and ± 8 dbar between 5°S and 5°N.

In addition to these measures of equatorial conditions, the zonal pressure gradient was computed around the equator for $\sigma_\theta = 25.0$ kg m^{-3}. This surface lies close to the regional pycnocline core and is near the core of the Equatorial Undercurrent (EUC; Plate 1). When sufficient subsurface temperature data were available at a given buoy, the acceleration potential at $\sigma_\theta = 25.0$ kg m^{-3} was computed relative to 500 dbar using a local mean θ-S relation from a CTD climatology [*Johnson and McPhaden,* 1999]. When equatorial buoy data were insufficient at a given longitude, the average of the 2°S and 2°N buoy data were substituted, and when those substitutions were not possible, either 2°S or 2°N buoy data were used alone. The equatorial zonal pressure gradient at $\sigma_\theta = 25.0$ kg m^{-3} was estimated using centered differences of the acceleration potential values at buoy longitudes, except at the ends of the array, where forward differences were applied.

3. Meridional-Vertical Zonal Velocity and Salinity Sections

Large changes associated with the El Niño–La Niña cycle were observed in the CTD/ADCP zonal velocity (Plate 1) and salinity (Plate 2) sections. Oversimplifying the seasonal cycle into a boreal spring or warm season (January to June) and a boreal fall or cold season (July to December), as suggested by equatorial Pacific sea surface temperature [*Reynolds and Smith,* 1995], suits the semiannual CTD/ADCP sampling and our purposes.

Weak La Niña conditions predominated in boreal fall 1996 (Figure 1). Surface-intensified westward flow was found about the equator across the basin (Plate 1) in the northern and southern branches of the South Equatorial Current (SEC) [*Reverdin et al.,* 1994]. The surface-intensified North Equatorial Countercurrent (NECC) flowed eastward between 4° and 9°N [*Wyrtki and Kilonsky,* 1984]. The EUC shoaled from west to east with magnitude peaking in the central Pacific [*Yu and McPhaden,* 1999]. The subsurface salinity maximum of the South Pacific Tropical Water (SPTW) strengthened to the south and west (Plate 2) [*Tsuchiya,* 1968; *Johnson and McPhaden,* 1999]. The strong salinity front within the pycnocline delineated where salty SPTW and fresh northern waters converged within the EUC. The isolated salinity maximum advected eastward within the EUC was apparent in the east as was the surface salinity minimum under the Intertropical Convergence Zone (ITCZ). The surface meridional salinity front between the fresh NECC and the salty northern branch of the SEC was present in the central Pacific. Observed fields at 140° and 125°W in September 1996 were likely influenced by tropical instability waves [*Halpern et al.,* 1988; *Flament et al.,* 1996]. In short, currents and salinity were near normal, as expected during a weak La Niña.

The onset of El Niño in boreal spring 1997 resulted in unusual conditions. Downwelling Kelvin waves (Figure 1a) excited by westerly wind bursts (Figure 1b) during the El Niño development [*McPhaden,* 1999] influenced the February sections at 95° and 110°W and the April sections at 125° and 140°W. Hence very large EUC velocities (exceeding 2 m s^{-1} at 125°W) were sampled (Plate 1), and the isolated salinity maximum was stronger than normal on the equator from 140° to 110°W (Plate 2). A weakened EUC from 165°E to 155°W was consistent with a locally weakened or nonexistent zonal pressure gradient within the pycnocline when those longitudes were surveyed (Figure 2). The EUC was distinct from near-surface eastward flow about the equator at these longitudes. This transient surface current is an intermittent feature of the circulation driven by anomalous westerly equatorial winds (Figure 1b) and is referred to as the Eastward Equatorial Current (EEC), following *Delcroix et al.* [1992]. The NECC was unusually strong and south of its normal position for boreal spring, consistent with changes expected during a strong El Niño [*Taft and Kessler,* 1991]. Eastward flow predominated in the upper water column, with the SEC found only south of 2°S. An unusual tongue of salty water between the mixed layer and the pycnocline core extended northward from the equator to 4°–6°N between 165°E and 155°W. Since there is little zonal salinity gradient in the central equatorial Pacific, this tongue probably resulted from an extension of STPW influence northward across the equator as the pycnocline flattened out during El Niño [*Delcroix et al.,* 1992]. The northward spread was allowed by weakened geostrophic meridional convergence as illustrated by the weakened zonal pressure gradient (Figure 2).

The height of El Niño during boreal fall 1997 presented more unusual conditions. The NECC was again unusually strong and south in location (Plate 1). However, a month of near-normal easterly winds across much of the equatorial Pacific in July (Figure 1b) resulted in a temporary shoaling of the equatorial pycnocline in August (Figure 1a). As might be expected, the northern branch of the SEC and a strong southern branch were evident only in August, along 95° and 110°W. Surface freshening and a deep pycnocline across the basin suggested an absence of equatorial upwelling, contrasting strongly with the preceding and following boreal falls (Plate 2 and Figure 1a). An especially large freshening occurred about the equator over the warm

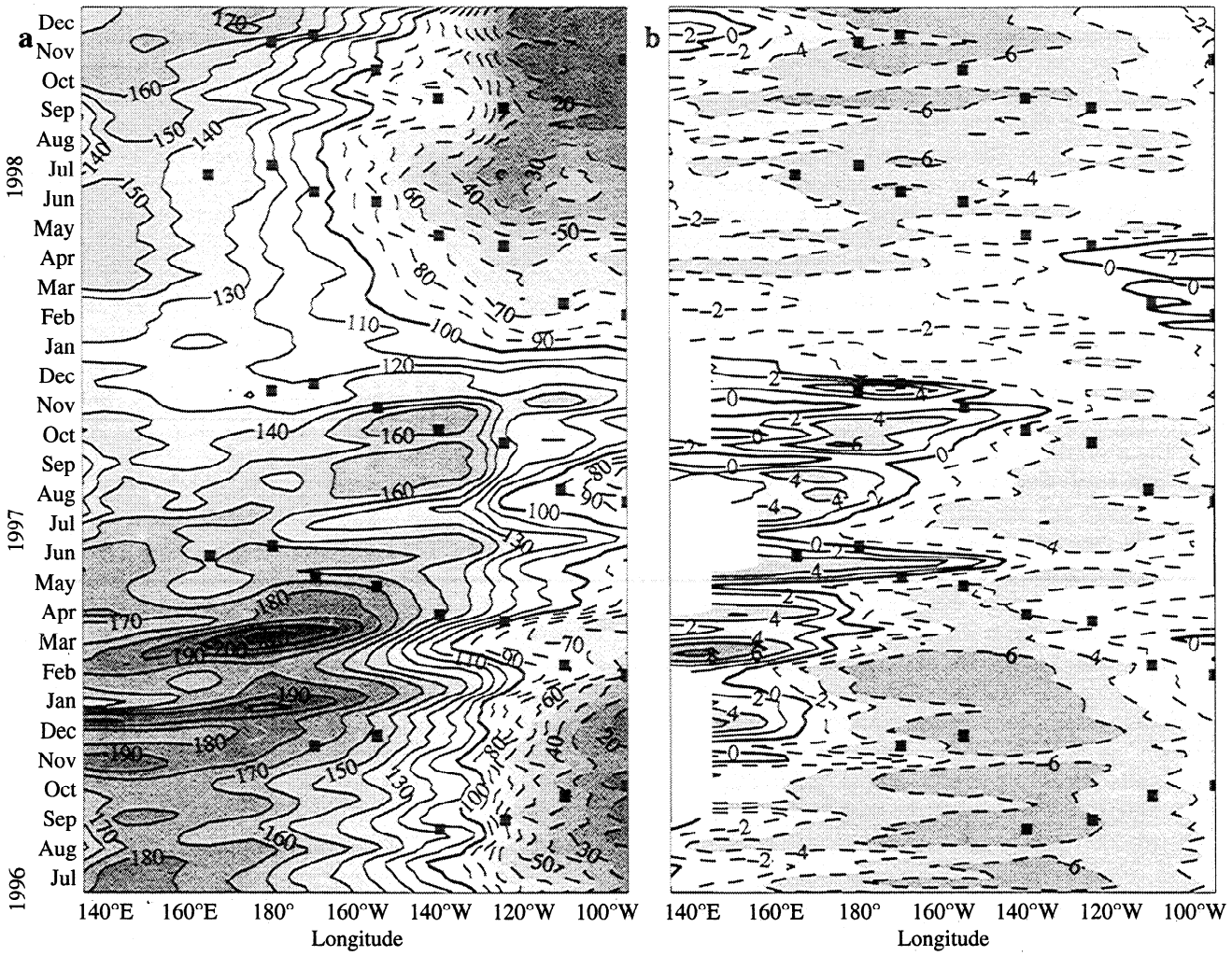

Figure 1. CTD/ADCP section longitude and time (small solid rectangles) superimposed on (a) contours of 5-day average equatorial 20°C isotherm depth (10 m intervals where solid contours are deeper than 100 m, dashed contours are shallower than 100 m, contours are thick at 100 m intervals, and darker shading is farther from 100 m) and (b) contours of 5-day average zonal winds (2 m s^{-1} intervals where solid contours are westerlies, dashed contours are easterlies, the zero contour is thick, and darker shading is farther from zero). Both quantities are from the Tropical Atmosphere-Ocean (TAO) moored buoy array.

pool from 180° to 155°W (<34.0 at 155°W). This freshening could not have been solely due to eastward advection [*Delcroix and Picaut,* 1998] because water this fresh was not seen to the west during the previous season (Plate 2). Thus increased local precipitation during the El Niño is implicated [*Ando and McPhaden,* 1997]. In addition, some of this fresher water could have been advected south because of near-surface equatorial Ekman convergence driven by the anomalous westerly winds about the equator (Figure 1b). Surface freshening was also large north of the equator under the ITCZ at 140° and 125°W. The EUC was quite weak, consistent with the weakening and even reversal of the zonal pressure gradient in the pycnocline (Figure 2), and a complex zonal current structure was evident near the equator from 180° to 140°W. The weak EUC and an EEC were separated by reduced eastward flow and even some westward flow, especially at 155°W. This upper ocean structure was probably a transient ocean response to westerly wind bursts (Figure 1b), similar to reversing jets sometimes observed farther west [*McPhaden et al.,* 1992; *Cronin et al.,* 2000]. Over the same longitudes the equatorial salinity front within the pycnocline was much weaker than boreal fall 1996, with a tongue of salty SPTW between the mixed layer and the pycnocline core extending as far as 6°N. Between 180° and 155°W the meridional salinity gradient from 1°S to 1°N on σ_θ = 25 kg m^{-3} was reduced to one third of its value for the previous and following seasons. These features were again likely due to reduced equatorward geostrophic convergence [*Delcroix et al.,* 1992]. In fact, the zonal pressure gradient reversal even suggested some poleward geostrophic divergence within the pycnocline at times during this El Niño (Figure 2).

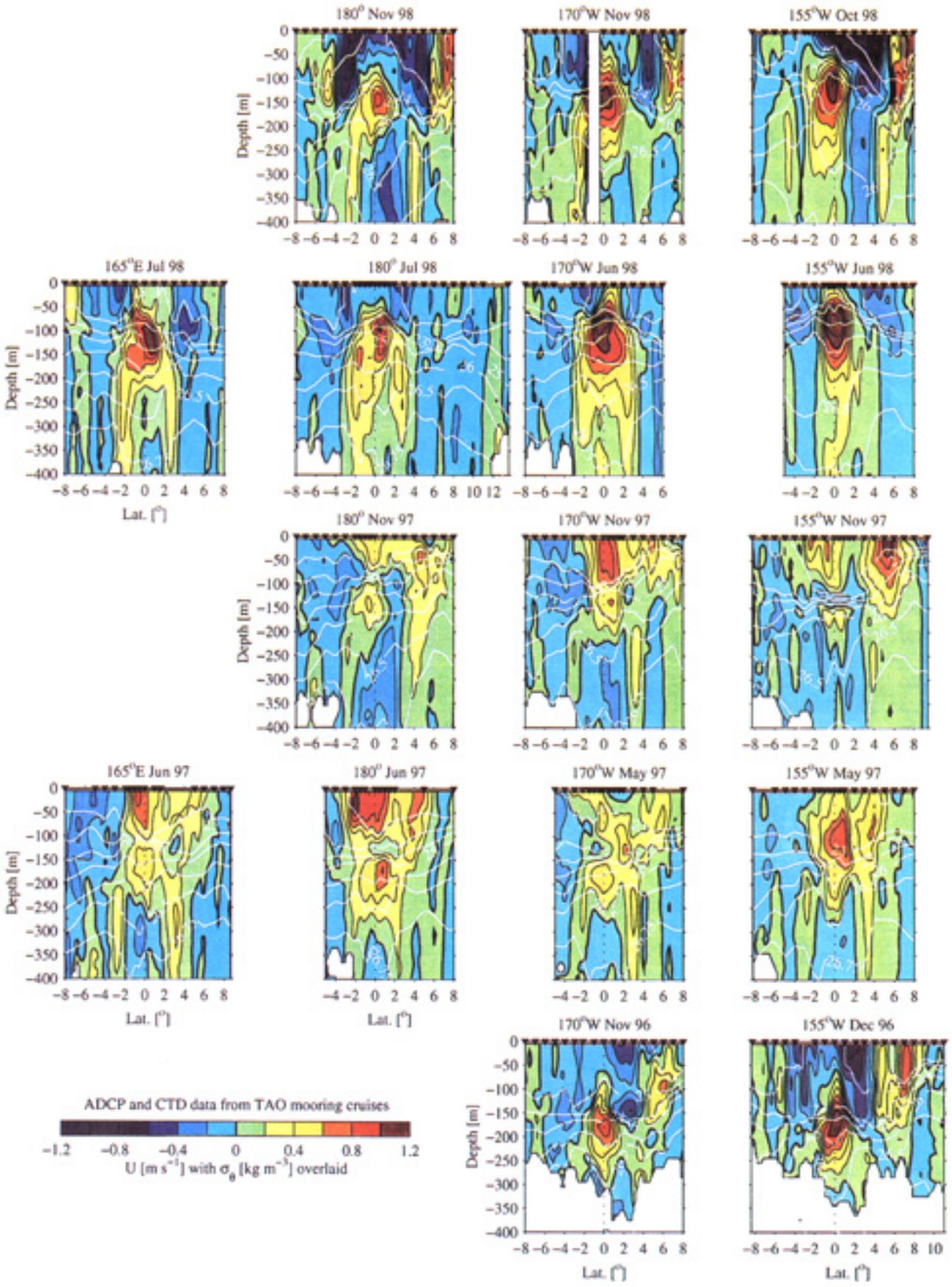

Plate 1. Meridional-vertical sections of acoustic Doppler current profiler (ADCP) zonal velocity (U; at 0.2 m s^{-1} intervals; color bar) with potential isopycnals (σ_θ; at 1 kg m^{-3} intervals lighter than 26 kg m^{-3} and 0.25 kg m^{-3} intervals denser than 26 kg m^{-3}; white). Longitudes are columns, and seasons are rows. Conductivity-temperature-depth (CTD) station locations (triangles) vary.

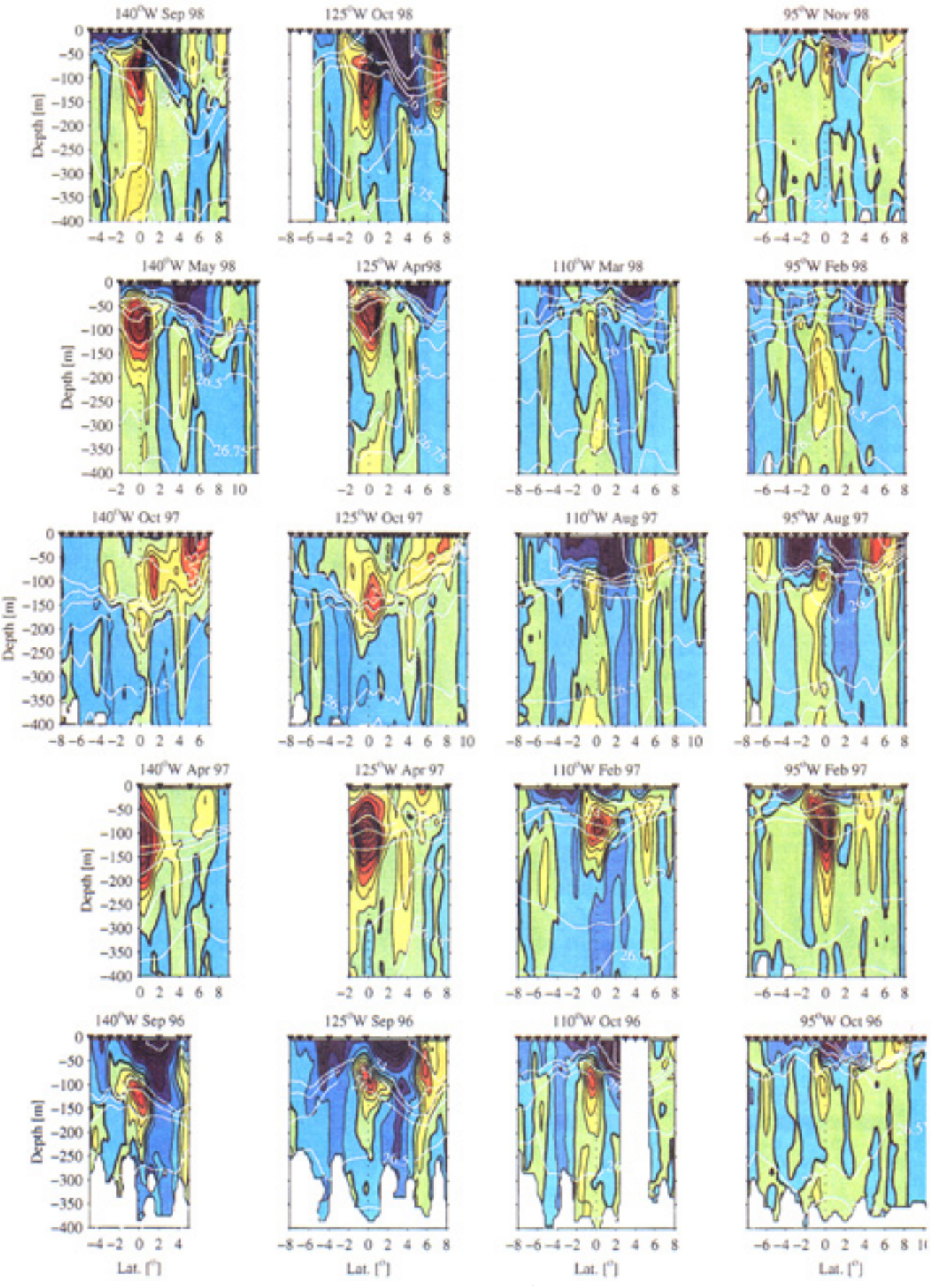

Plate 1. (Continued)

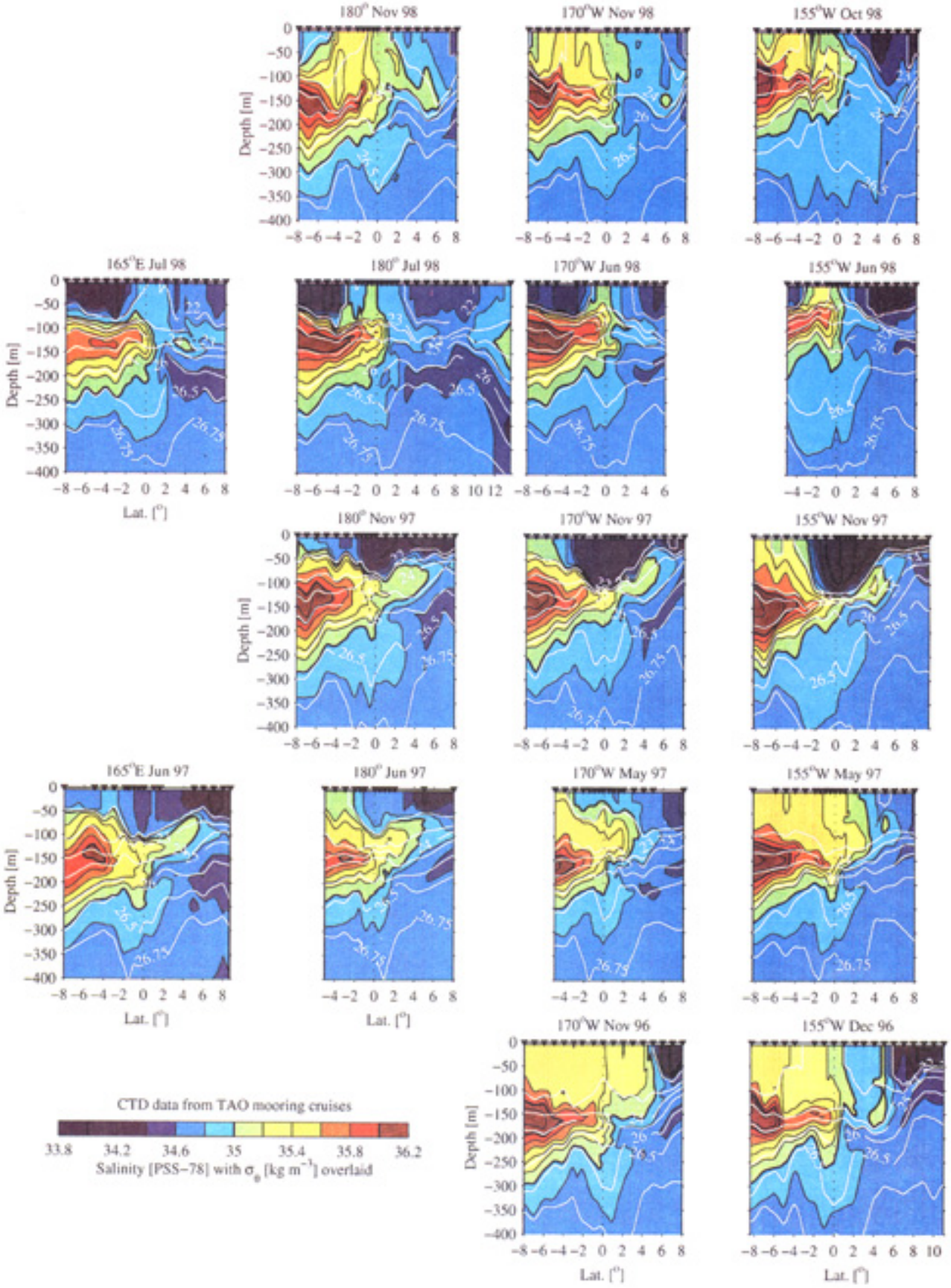

Plate 2. As in Plate 1 but for meridional-vertical sections of CTD salinity (S; at 0.2 intervals, color bar) with potential isopycnals (σ_θ, white).

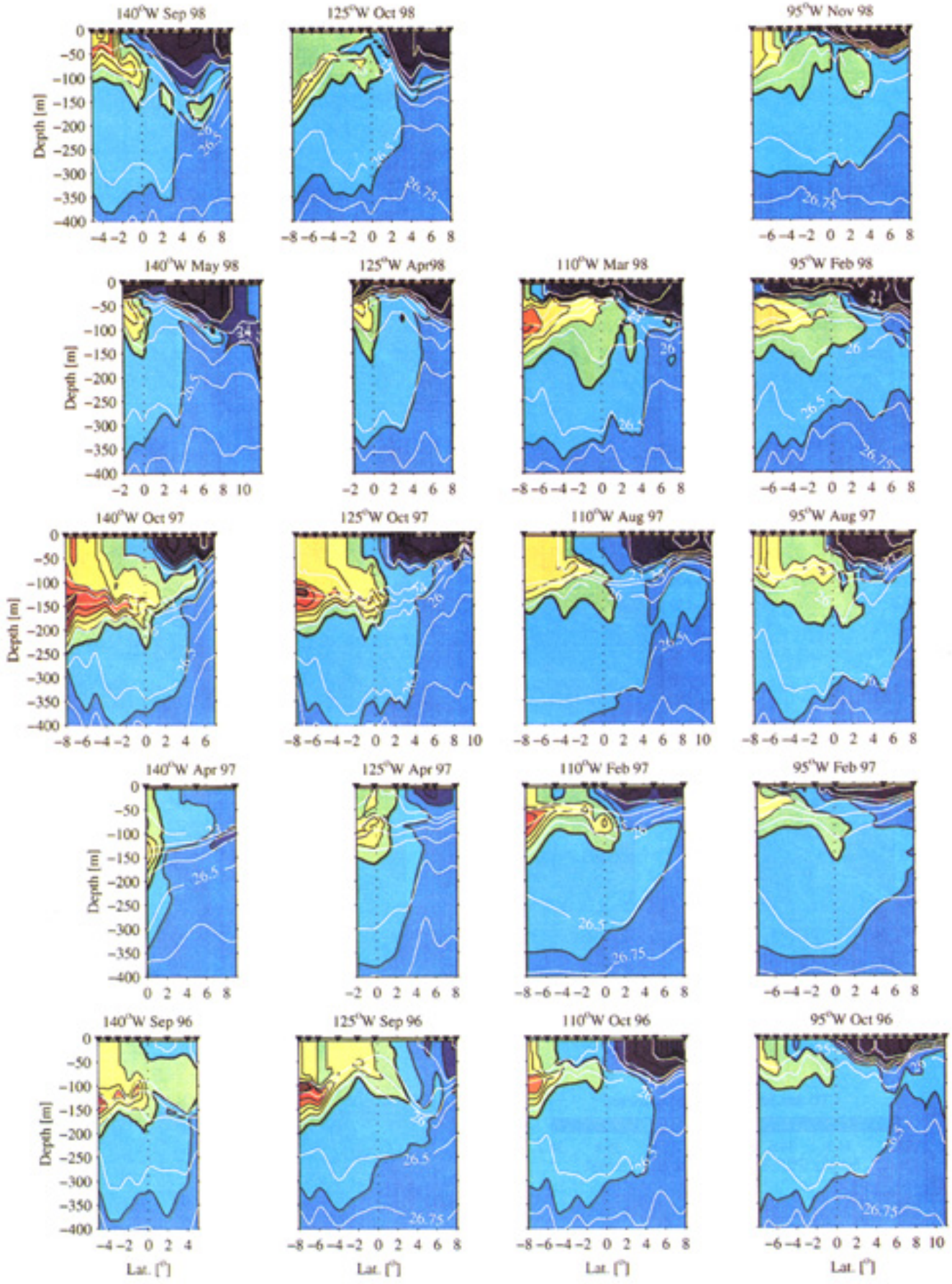

Plate 2. (Continued)

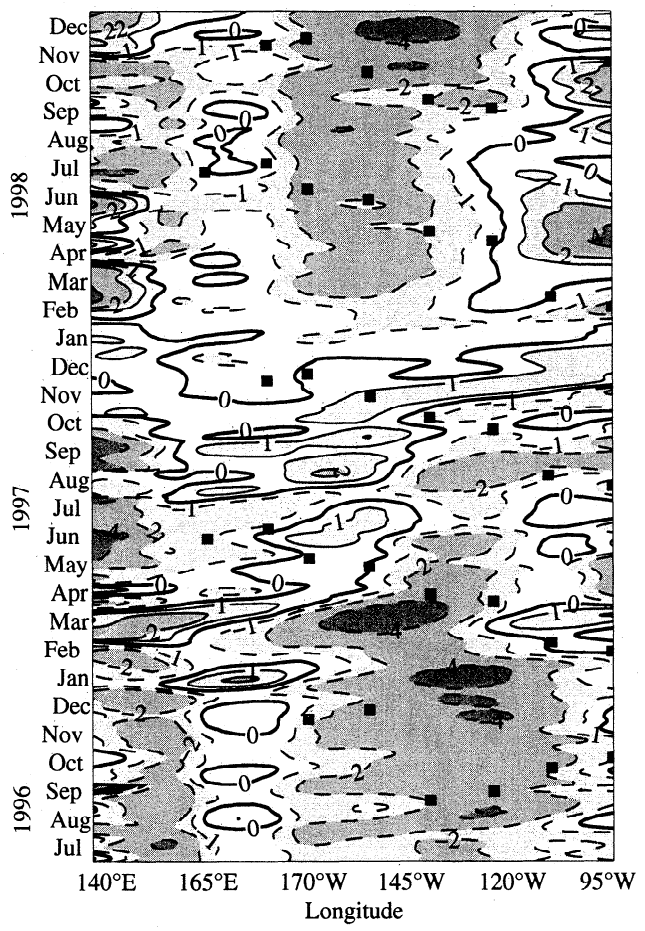

Figure 2. CTD/ADCP section longitude and time (small solid rectangles) superimposed on contours of equatorial zonal pressure gradient on $\sigma_\theta = 25.0$ kg m^{-3} relative to 500 dbar (contours at 0, ±1, ±2, ±4, and ±8 $\times 10^{-4}$ N m^{-3}, where dashed contours are negative, the zero contour is thick, and darker shading is farther from zero). The quantity is derived from the TAO moored buoy array and local mean θ-S relations from a CTD climatology [*Johnson and McPhaden*, 1999] and has been smoothed with a 10-day half-width Hanning filter.

While it is not obvious from Plate 2, from 125° to 95°W, salinities were high between the mixed layer and pycnocline core in both hemispheres. Unlike in the central Pacific, salinity decreases to the east here, so some of this change could have been due to anomalous eastward flow with the relaxation of the SEC, the appearance of the EEC, and the strong NECC.

During the decay phase of the El Niño and the transition to La Niña in boreal spring 1998 conditions changed again. The SEC became strong on both sides of the equator across the basin (Plate 1), as expected during La Niña [*Frankignoul et al.*, 1996]. The NECC weakened, as is usual during this season, and, where present at all, appeared very far north, as is usual after a strong El Niño [*Taft and Kessler*, 1991]. In March the pycnocline was still deep (Figure 1a), and the abrupt disappearance of anomalous warm sea surface temperatures had not yet occured [*McPhaden*, 1999]. Thus, in the March sections at 110° and 95°W the EUC was weak, the surface water was fresh (Figure 2), probably because of anomalously strong precipitation affecting the eastern equatorial Pacific at this time [*McPhaden*, 1999], and anomalous salty water was again found between the pycnocline and the mixed layer. The EUC was very strong in the other sections occupied from April through July after the return of easterly winds (Figure 1b), the development of a shallow pycnocline in the east (Figure 1a), and the reestablishment of an eastward zonal pressure gradient within the central Pacific pycnocline (Figure 2). Consonant with the renewal of equatorward geostrophic convergence, the equatorial salinity front in the pycnocline sharpened again with the SPTW influence reduced north of the equator between 165°E and 155°W. While surface salinities remained fresh overall, a chimney of salty water extended to the surface on the equator in this longitude range, clearly indicating resumed upwelling. The equatorial pycnostad was significantly reduced at 95°W, similarly to the period after the 1982–1983 El Niño [*Hayes et al.*, 1987], and the Subsurface Countercurrents (SCCs) [*Rowe et al.*, 2000; *Johnson and Moore*, 1997; *Tsuchiya*, 1975], both north (NSCC) and south (SSCC), normally found on either side of the pycnostad, all but disappeared at that longitude.

Strong La Niña conditions prevailed in boreal fall 1998. The SEC, EUC, and associated equatorial salinity front were stronger everywhere save 95°W (Plates 1 and 2), and the pycnocline shoaled significantly with respect to the previous boreal fall. The NECC was also generally strong. Uplifted isopycnal and isohalines were again suggestive of equatorial upwelling, especially from 180° to 155°W, with dense salty water being drawn up from below. Surface salinities increased toward normal values at 180° and 170°W, probably from some combination of upwelling, horizontal advection, and reduced precipitation. The earlier surface freshness appeared to have mixed down into both branches of the SEC from 155° to 125°W, greatly reducing the salinity maximum of the SPTW.

4. Zonal Volume Flux Variability

Large volume transport changes from mid-1996 through 1998 were revealed by a quantitative evaluation of the time-varying zonal circulation in the upper equatorial Pacific Ocean using the section data. Zonal volume transports were estimated for two layers. The upper layer extended from the surface to the pycnocline core at $\sigma_\theta = 24.25$ kg m^{-3}, the regional average buoyancy frequency maximum. This upper layer (Figure 3 and Table 1) captured most of the surface current (SEC, NECC, and EEC) zonal transports and sometimes a small fraction of the EUC transport. The lower layer contained water of 24.25 kg m^{-3} $< \sigma_\theta <$ 26.5 kg m^{-3}. The denser bounding isopycnal was near the

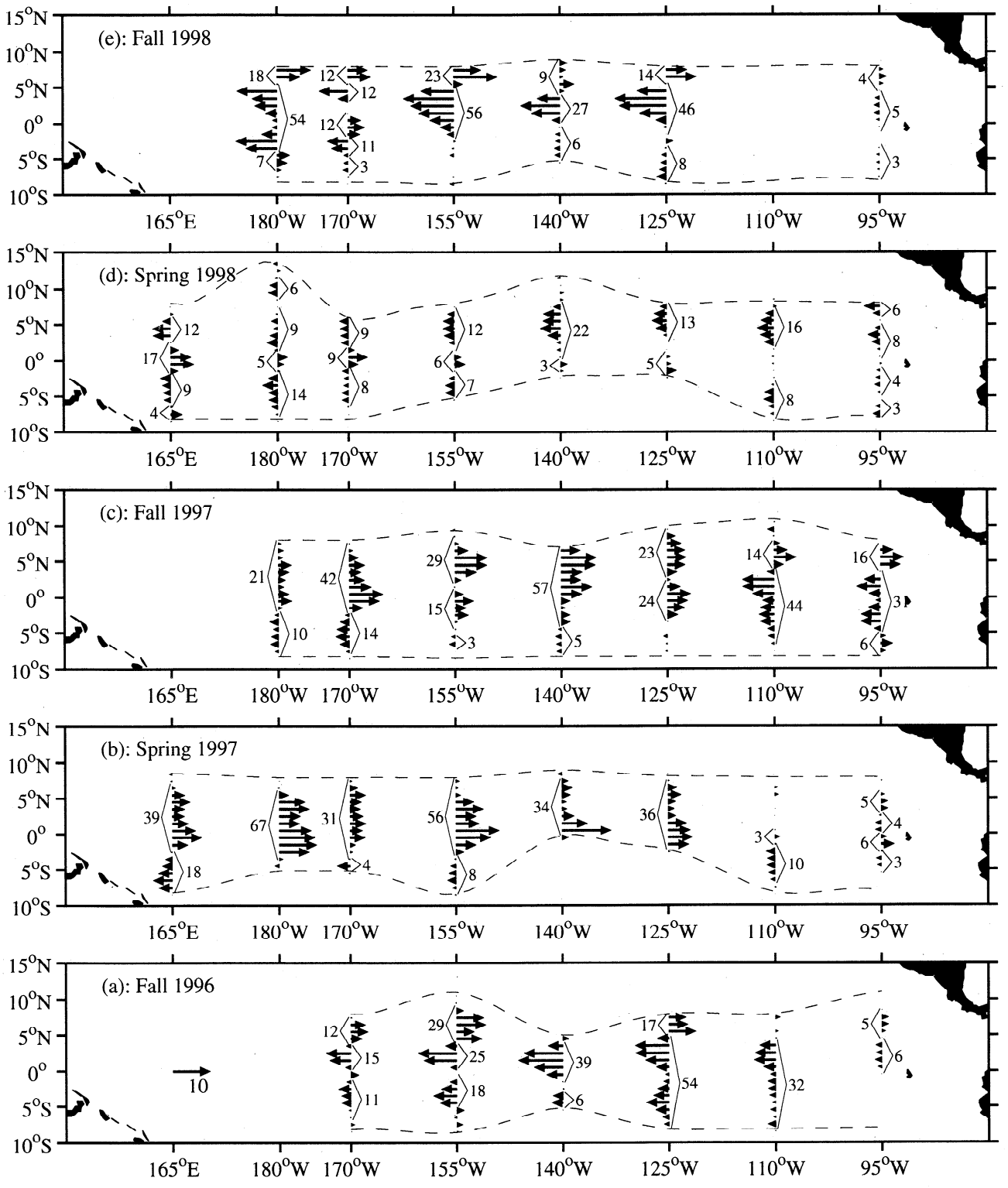

Figure 3. Zonal volume transport (10^6 m^3 s^{-1}) for the upper layer water with $\sigma_\theta < 24.25$ kg m^{-3}. Seasons progress upward from (a) boreal fall 1996 through (e) boreal fall 1998. Arrows are proportional to layer-averaged transport over 1° latitude intervals, with a key in Figure 3a. Brackets delineate unidirectional layer transport latitude ranges of magnitude $>2 \times 10^6$ m^3 s^{-1}. Numbers adjacent to the brackets are net integrated transports over those ranges. Dashed lines show the latitudinal ranges of the sections.

Table 1. Seasonal Means and Standard Deviations of Layer Zonal Current Volume Transports

	Upper Layer Zonal Current Volume Transports, 10^6 m^3 s^{-1}		
Boreal Season	SEC	NECC & EEC	EUC
Fall 1998	-38 ± 20^a	13 ± 7^a	2 ± 5^a
Spring 1998	-22 ± 5^b	—	6 ± 6^b
Fall 1997	-6 ± 6^c	42 ± 13^c	—
Spring 1997	-12 ± 5^d	46 ± 15^e	—
Fall 1996	-34 ± 17^f	13 ± 11^g	—
	Lower Layer Zonal Current Volume Transports, 10^6 m^3 s^{-1}		
Boreal Season	SEC	NECC (& NSCC)	EUC (& SCCs)
Fall 1998	-8 ± 13^a	5 ± 4^a	34 ± 17^a
Spring 1998	-13 ± 6^b	—	35 ± 18^b
Fall 1997	-11 ± 4^c	18 ± 5^c	
Spring 1997	-9 ± 6^d	24 ± 5^h	
Fall 1996	-15 ± 14^f	5 ± 4^g	16 ± 8^f

SEC, Southern Equatorial Current; NECC, North Equatorial Countercurrent; EEC, Eastward Equatorial Current; EUC, Equatorial Undercurrent; NSCC, North Subsurface Countercurrent; and SCC, Subsurface Countercurrents.

[a]180°–95°W.

[b]165°E–95°W, excluding 140° and 125°W from the southern branch of the SEC.

[c]180°–125°W, combining NECC and EUC estimates.

[d]165°E, 155°W, and 110°W.

[e]165°E–125°W, excluding 140°W.

[f]170°W–95°W.

[g]170°W–95°W, excluding 140°W.

[h]165°E–155°W, combining NECC and EUC estimates.

deep equatorial pycnostad associated with 13°C water. Transports in the lower layer (Figure 4 and Table 1) captured the bulk of the EUC and some of the SCCs as well as deep expressions of the surface currents (a fraction of their near-surface flow). Layer transports were again grouped into 6-month spring and fall intervals for discussion. While there were often coherent patterns across much of the basin in a given season, it is important to remember that sets of synoptic sections occupied over 6-month seasons are susceptible to aliasing over a wide variety of timescales.

Reversals in layer-integrated transport defined the meridional boundaries for currents. Net volume transports between these current boundaries are given at each longitude (Figures 3 and 4). Seasonal summaries of the transports (Table 1) included those sections that appeared to sample fully the current in question but excluded the 1997 eastern Pacific sections for reasons given below. Also, during 1997 the absence of the northern branch of the SEC precluded separation of the NECC from the EEC in the upper layer and the NECC from the EUC in the lower layer, so combined transports for these currents were reported (Table 1).

Weak La Niña conditions prevailed in boreal fall 1996. Both branches of the SEC were strong, as was the NECC from 170° to 125°W, where sections extended far enough north to sample it (Figures 3a and 4a and Table 1). The EUC was clearly evident in the lower layer, with transports decreasing from 170° to 95°W.

The onset of El Niño in boreal spring 1997 resulted in dramatic volume transport changes (Figures 3b and 4b and Table 1). The northern branch of the SEC vanished, and the southern branch was weak where sampled from 165°E to 110°W. Overall, SEC transport was less than half the previous season's value. Unexpectedly for boreal spring but characteristically for El Niño [*Taft and Kessler*, 1991], the NECC was robust; a strong EEC had also appeared (Plate 1). These currents combined to give net eastward upper layer transport $>40 \times 10^6$ m^3 s^{-1}. The EUC weakened west of 140°W, consistent with weakening or elimination of the equatorial zonal pressure gradient in the pycnocline (Figure 2). Sections from 140° to 95°W were occupied coincident with the progression of a pair of equatorial Kelvin waves (Figure 1a), so very large eastward velocities (Plate 1) and lower layer transports (Figure 4b) were found about

the equator. These conditions were transient and did not reflect the EUC transport over seasonal timescales. (Moored ADCP time series from the TAO array support this statement.) The El Niño was not yet underway when the two easternmost sections were taken. Hence eastern Pacific sections were not included in this season's transport estimates (Table 1).

The persistence of El Niño into boreal fall 1997 was reflected in the layer transports (Figures 3c and 4c and Table 1). Again, only a weak southern branch of the

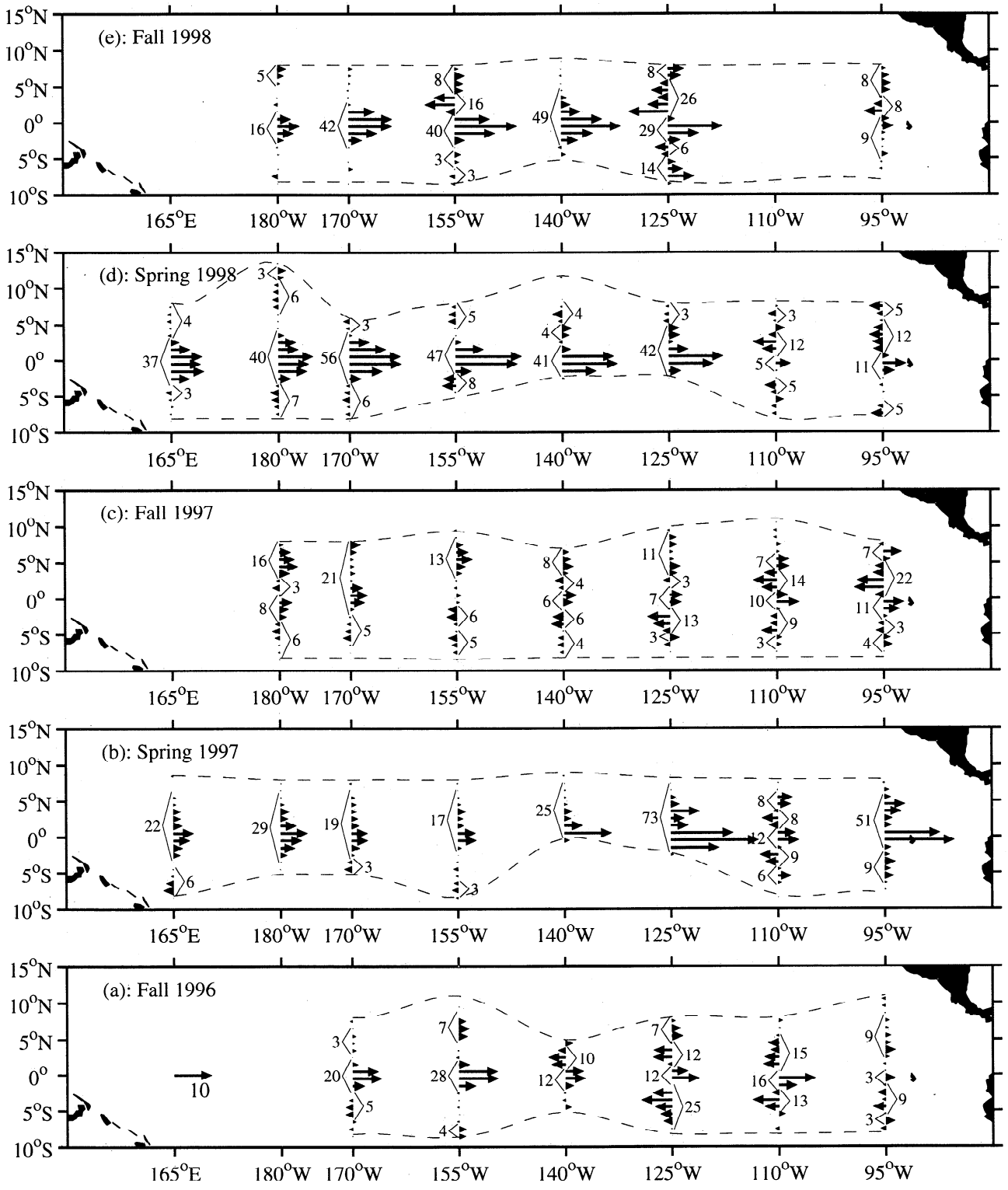

Figure 4. As in Figure 3 but for zonal volume transport (10^6 m^3 s^{-1}) for the lower layer water with 24.25 kg m^{-3} $< \sigma_\theta <$ 26.5 kg m^{-3}.

SEC was evident between 180° and 140°W. As expected for the boreal fall, the NECC strengthened, but the EEC was weaker (Plate 1). Their combined upper layer transport had similar size to the previous season (Table 1). The EUC was weak in the lower layer, and the flow north of the southern branch of the SEC was not uniformly eastward, summing to a small net eastward transport between 180° and 125°W. The very weak EUC (Plate 1) was doubtlessly related to the remarkably flat pycnocline (Figure 1a) and weak or even reversed zonal pressure gradient (Figure 2) at the time. The eastern Pacific again differed from the rest of the basin and was excluded from the transport estimates for this season (Table 1). Transports in the east were exceptional because in July 1997, 1 month prior to when the sections at 110°W and 95°W were taken, zonal equatorial winds were easterly across much of the Pacific (Figure 1) and, so, nearer to normal than during the rest of the El Niño. Thus, in contrast to the rest of the basin (Table 1), the NECC in the east carried $15 \pm 1 \times 10^6$ m^3 s^{-1}, and the SEC carried $-38 \pm 9 \times 10^6$ m^3 s^{-1}, consistent with the near-normal wind conditions. In the east the lower layer transport alternated sign from the SSCC to the southern branch of the SEC to the EUC to the northern branch of the SEC to the NSCC and NECC. Net zonal transport integrated across these alternating flows was not significantly different from zero.

The transition toward La Niña was evident in the layer transports for boreal spring 1998 (Figures 3d and 4d and Table 1). The SEC was present consistently on both sides of the equator between 165°E and 95°W. No significant NECC transport was found in any of these sections; its absence across the entire basin seems extraordinary even for boreal spring. The EUC returned and was robust between 165°E and 95°W, generally decreasing in transport from west to east. The EUC was also evident in the upper layer across much of the basin. In contrast to the previous two seasons, the section at 95°W reveals the same currents as those to the west, but generally weaker.

A strong La Niña was clearly indicated in the layer transports (Figures 3e and 4e and Table 1) for boreal fall 1998. The SEC was present in all the sections, and its transport nearly doubled compared to the previous season. As expected for boreal fall, the NECC was robust. The EUC was quite strong but induced eastward upper layer transport only at 170°W. Again, the section at 95°W revealed weaker versions of currents to the west.

These large volume transport changes reflected interannual variability associated with the El Niño–La Niña cycle. Summing estimates in both layers (Table 1), westward transport in the SEC was as high as $49 \pm 22 \times 10^6$ m^3 s^{-1} in boreal fall 1996 and as low as $17 \pm 7 \times 10^6$ m^3 s^{-1} in boreal fall 1997. Eastward transport in the combined NECC, EEC, EUC, and SCCs ranged from as low as $34 \pm 14 \times 10^6$ m^3 s^{-1} in boreal fall 1996 to as high as $70 \pm 16 \times 10^6$ m^3 s^{-1} in the following season. Net transports integrated across the low-latitude currents in both layers ranged from $15 \pm 26 \times 10^6$ m^3 s^{-1} westward in boreal fall 1996 to $49 \pm 18 \times 10^6$ m^3 s^{-1} eastward in the following season, a net change roughly the size of a hypothetical reversal of the Florida Current.

5. Zonal Transports and Warm-Water Volume Changes

The large variability in equatorial upper ocean zonal transports was related to regional volume changes of near-equatorial warm water following *Delcroix et al.* [1992]. Salinity data are much scarcer than temperature data in the upper equatorial ocean, so instead of the previous isopycnal boundary separating upper ocean water from that at depth, the 20°C isotherm was used, following *Kessler* [1990]. The 5°S to 5°N interval was characterized by current reversals and significant thermocline depth variability and was sampled by 30 out of the 35 CTD/ADCP sections. Hence the volume of water above the 20°C isotherm between 5°S and 5°N was derived from TAO array data (extrapolating to the boundaries using isotherm slopes between the outermost buoy pairs at each end of the array). The time series at each longitude were smoothed using a 25-day half-width Hanning filter to reduce the influence of tropical instability waves and other transients. The results were then integrated zonally in both directions to obtain volumes of near-equatorial warm water to both the east and the west of all longitudes.

Time derivatives of the near-equatorial warm-water volumes to the west of any given longitude volumes revealed the need for net transports that exceeded 50×10^6 m^3 s^{-1} on intraseasonal to interannual timescales to balance the volume changes (Figure 5). The volume budget contours and the observed values computed from each section (Figure 5) showed a general correspondence of measured zonal transports and total transports required from the volume budget to the west. The comparison was incomplete because meridional transports across the bounding latitudes, volume exchange with the Indian Ocean via the Indonesian Throughflow, and diabatic transports across the bounding 20°C isotherm were not taken into account. However, our aim was not a complete mass balance (as considered by C. S. Meinen and M. J. McPhaden (Warm water displacements in the equatorial Pacific during 1993–1999, submitted to *J. Phys. Oceanogr.*, 1999)) but an examination of one important aspect of ENSO variability: the zonal redistribution of warm upper ocean water along the equator. In particular, we explored relationships between the CTD/ADCP section warm-water transports and the temporal changes in warm-water volumes.

The CTD/ADCP transports and the warm-water volume budget to their west were compared directly in a scatter plot (Figure 6). Their correlation coefficient was 0.73. Were each CTD/ADCP transport measurement

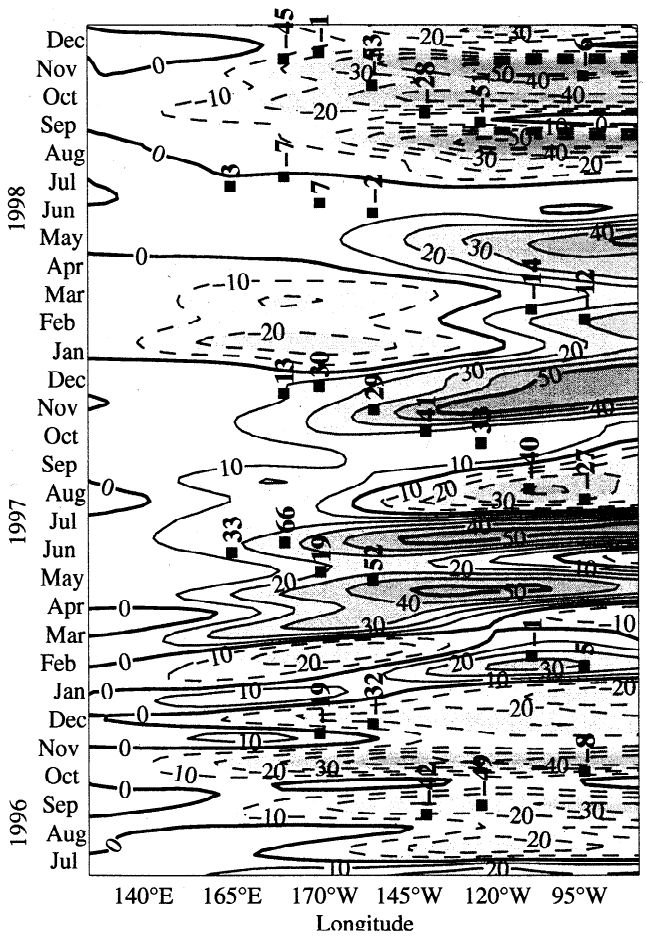

Figure 5. Zonal transport (10×10^6 m^3 s^{-1} intervals where solid contours are positive, dashed contours are negative, contours are thick at 50×10^6 m^3 s^{-1} intervals, and darker shading is farther from zero) inferred by the rate of change of volume integrated from the western boundary above 20°C from 5°S to 5°N filtered with a 25-day half-width Hanning filter. Volume transports over the same range (10^6 m^3 s^{-1} in vertical bold face type) for CTD/ADCP sections are given above their longitudes and times (small solid rectangles).

independent, 30 degrees of freedom would result. However, the integral timescales and length scales estimated from the warm-water volume budget (Figure 5) were 91 days and 60° longitude. Using the very conservative estimate of 11 degrees of freedom for the 819 days and 100° longitude sampled, the correlation was still significant to 99%. An orthogonal least squares estimate of the ratio of inferred to measured transports was 0.63 ± 0.10 (Figure 6). The standard error was estimated by the jackknife technique [*Efron,* 1982]. Restating this, measured CTD/ADCP transports were approximately 1.6 times those inferred from the volume budget. This result is somewhat different from *Delcroix et al.* [1992], who found a relation near unity. However, it should be noted that they presented their results without an error budget and integrated the observed transport measurements rather than time differentiating the warm-water volume to make their comparison.

Our result has at least two possible explanations. First, if the measured zonal transports balanced the transports inferred from changes in volume of the warm water but the synoptic CTD/ADCP transport estimates contained considerable high-frequency noise, the ratio of inferred to measured transports would be reduced from unity. For instance, if the CTD/ADCP transports had normally distributed noise-to-signal ratio of 0.92, this would lead to a correlation coefficient of 0.73 ± 0.09 and a ratio of 0.67 ± 0.12, similar to the results above. However, given the general consistency of the upper water zonal transports over 6-month periods across much of the basin (Figure 3), it seems unlikely that noise in the CTD/ADCP transport estimates was large enough to be the sole cause of the low ratio.

A second explanation is suggested by considering linear reduced gravity simulations forced by observed winds [*Zebiak,* 1989]. In this model, upper ocean volume changes in warm water during all phases of an ENSO cycle were opposed by meridional transports at the western boundary but enhanced somewhat by interior meridional transports. The result of this tendency was that near-equatorial zonal warm-water volume transports in the model were greater than those required to account for warm water volume changes, especially in the western and central Pacific. To look for this tendency, we estimated ratios and correlation coefficients separately in the western, central, and east-

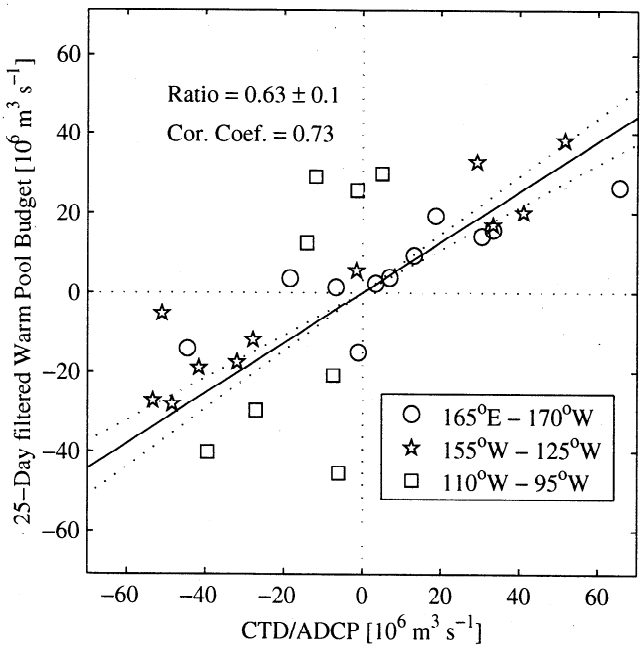

Figure 6. Scatterplot of CTD/ADCP section equatorial warm-water transports (above 20°C from 5°S to 5°N) versus transports required to balance temporal changes in the volume of the warm water over the same range to the west of each section. The slope of the orthogonal least squares fit is 0.63 ± 0.10 with a correlation coefficient of 0.73. The legend shows which symbols correspond to the western, eastern, and central Pacific.

ern regions (Figure 6). The ratios increased from 0.43 ± 0.05 to 0.53 ± 0.08 to 2.7 ± 3.3, respectively, in these regions. The correlation coefficients were 0.85, 0.94, and 0.59, which, assuming 5, 6, and 5 degrees of freedom, were significant to 93%, 99%, and 71%, respectively. The ratio of measured zonal transports to those inferred from a warm-water budget to the west increased to the east, consistent with the model results.

Transports inferred from a volume budget integrated westward from the eastern boundary (not shown) had a more tenuous relation to measured transports. The overall comparison gave a correlation coefficient of –0.04 and a ratio of –0.03 ± 0.13, only a 9% probability of significant correlation assuming 11 degrees of freedom. Making separate fits to data in the western, central, and eastern regions (not shown) again allowed some insight, giving ratios of –0.70 ± 0.73, 0.08 ± 0.08, and 0.50 ± 0.21, respectively. The correlation coefficients were –0.41, 0.43, and 0.75, which, assuming 5, 6, and 5 degrees of freedom, are significant to 51%, 61%, and 86%, respectively. The relation in the easternmost region was the closest to being significant, with measured transports roughly twice those inferred from the eastern volume budget. As in the case of the volume budgets integrated from the western boundary, this ratio implies a significant meridional convergence or divergence of warm water in the eastern Pacific tending to counterbalance zonal volume transports during 1996–1998.

The thermocline undergoes an overall deepening while its slope increases during La Niña and vice versa during El Niño [*Jin,* 1997]. The high correlation of measured transports with the volume budget to the west and low correlation with the volume budget to the east may have resulted from this pattern. Constructive interference of depth and slope in the west would tend to allow high correlations of zonal volume transports with a western volume budget, while destructive interference in the east would tend to reduce correlations with an eastern volume budget. To test this hypothesis, variations of the mean thermocline depth were removed from both volume budgets to explore the relation of changes in the thermocline slope to the zonal equatorial warm-water transport (not shown). The overall correlation was near 0.67 for either direction of integration, and the ratio of inferred to measured transports was reduced to 0.25 ± 0.05. The ratios and correlations for these budgets were between the results for the overall eastern and western budgets. This result supported the hypothesis since removing one component of the thermocline variability should reduce the interference effects to both the east and the west.

6. Discussion

Very large changes in upper ocean currents over interannual and shorter timescales were revealed by the CTD/ADCP sections and the moored measurements from the TAO buoys. The section data provided a geographically broad, spatially high-resolution sampling of upper ocean currents during the most recent ENSO cycle, a view unavailable for previous Los Niños and Las Niñas, for which shipboard data were much more temporally and geographically limited. TAO buoy data provided temporal continuity of basin-wide equatorial wind and subsurface temperature fields. The disappearance or near disappearance of the EUC was previously observed where data were available at individual longitudes during previous Los Niños [*Firing et al.,* 1983; *Halpern,* 1987; *McPhaden et al.,* 1990; *Kessler and McPhaden,* 1995]. During the 1997–1998 El Niño the shipboard measurements showed that the EUC virtually disappeared across much of the basin, associated with the weakening or even the reversal of the equatorial zonal pressure gradient within the pycnocline. As well, development of the EEC in response to westerly wind bursts was observed over a greater longitude range than in data from 1989 and 1990 [*McPhaden et al.,* 1992; *Kuroda and McPhaden,* 1993], and its disappearance with La Niña was also documented. These and other current changes, notably in the NECC and SEC, result in very large changes in zonal mass transport, as large as $64 \pm 32 \times 10^6$ m^3 s^{-1} over 6 months.

Significant changes in the upper ocean thermohaline fields were documented by the section data. During boreal fall 1997 in the central Pacific the meridional salinity gradient within the thermocline near the equator was about a third that in preceding and following seasons. This reduction was consistent with the zonal pressure gradient reversal and was larger than the 50% reduction reported at 165°E during the 1986–1987 El Niño [*Delcroix et al.,* 1992]. Salinity decreased to 34.0 in November 1997 in the upper 100 m on the equator at 155°W, which was roughly 0.4 lower than the lowest sea surface salinity measurements in the vicinity during the 1982–1983 El Niño [*Delcroix and Hénin,* 1991] and only 0.2 higher than the lowest values reported on the equator near 170°E in August 1997 [*Delcroix et al.,* 1998]. This remarkably thick fresh layer for the region [*Ando and McPhaden,* 1997] was partially due to equatorial downwelling through zonal and meridional convergence and a southward excursion of near-surface fresh water by anomalous southward Ekman drift, as seen during westerly wind bursts in 1989–1990 [*McPhaden et al.,* 1992; *Kuroda and McPhaden,* 1993]. In the eastern Pacific, anomalously salty water was found within the thermocline early in this event, as in the 1982–1983 El Niño [*Mangum et al.,* 1986], arguably the product of strong eastward advection. In the same region a strong near-surface halocline developed later in the event, similar again to the 1982–1983 [*Hayes et al.,* 1987] and the 1986–1987 events [*McPhaden and Hayes,* 1990].

Finally, equatorial zonal volume transports in the upper ocean were closely related to zonal shifts of warm-water volume, especially in the western Pacific, a result in rough accord with a similar budget for the water west of 165°E during 1984–1988 [*Delcroix et al.,* 1992]. The relationship between equatorial zonal upper ocean volume transport and volumetric changes to the east of the

sections was less clear, with marginally significant correlations found only for the eastern sections, in agreement with an eastern Pacific mass budget during the 1982–1983 El Niño [*Mangum et al.*, 1986]. The results from comparisons of measured and inferred transports were consistent with simple numerical [*Zebiak*, 1989] and conceptual [*Jin*, 1997] models of the ENSO cycle.

Acknowledgments. This work would not have been possible without data collected through careful and sustained work of the officers, crew, and scientific parties of the NOAA ships *Ka'imimoana* and *Ronald H. Brown*, especially Dennis Sweeney. Eric Firing's expertise and dedication ensured high-quality ADCP data collection, and June Firing ably processed most of those data. Dai McClurg made fields gridded from TAO buoy data easily available. Detailed constructive criticism from John Toole and comments from an anonymous reviewer improved the manuscript. This work was partially funded by the NOAA Office of Oceanic and Atmospheric Research, the NOAA Office of Global Programs, and the NASA Physical Oceanography Program. G.D.R. was supported by NOAA cooperative agreement NA67RJ0154. PMEL contribution 2093.

References

Ando, K., and M. J. McPhaden, Variability of surface layer hydrography in the tropical Pacific Ocean, *J. Geophys. Res., 102,* 23,063–23,078, 1997.

Bretherton, F. P., R. E. Davis, and C. B. Fandry, A technique for objective analysis and design of oceanographic experiments applied to MODE-73, *Deep-Sea Res. Oceanogr. Abstr., 23,* 559–582, 1976.

Cronin, M. F., M. J. McPhaden, and R. H. Weisberg, Wind forced reversing jets in the western equatorial Pacific, *J. Phys. Oceanogr.*, in press, 2000.

Delcroix, T., and C. Hénin, Seasonal and interannual variations of sea surface salinity in the tropical Pacific Ocean, *J. Geophys. Res., 96,* 22,135–21,150, 1991.

Delcroix, T., and J. Picaut, Zonal displacement of the western equatorial Pacific "fresh pool," *J. Geophys. Res., 103,* 1087–1098, 1998.

Delcroix, T., G. Eldin, M. H. Radenac, J. Toole, and E. Firing, Variations of the western equatorial Pacific Ocean, 1986–1988, *J. Geophys. Res., 97,* 5423–5445, 1992.

Delcroix, T., L. Gourdeau, and C. Hénin, Sea surface salinity changes along the Fiji-Japan shipping track during the 1996 La Niña and 1997 El Niño period, *Geophys. Res. Lett., 25,* 3169–3172, 1998.

Efron, B., *The Jackknife, the Bootstrap, and Other Resampling Plans, CBMS-NSF Reg. Conf. Ser. Appl. Math.*, vol. 38, 92 pp., Soc. for Ind. and Appl. Math., Philadelphia, Pa., 1982.

Firing, E., *Acoustic Doppler Current Profiling Measurements and Navigation, WHP Off. Rep. WHP091-1, WOCE Rep. 68/91,* 24 pp., Woods Hole Oceanogr. Inst., Woods Hole, Mass., 1992.

Firing, E., R. Lukas, J. Sadler, and K. Wyrtki, Equatorial undercurrent disappears during 1982–83 El Niño, *Science, 222,* 1121–1122, 1983.

Flament, P., S. Kennan, R. Knox, P. Niiler, and R. Bernstein, The three-dimensional structure of an upper ocean vortex in the tropical Pacific Ocean, *Nature, 383,* 610–613, 1996.

Frankignoul, C., F. Bonjean, and G. Reverdin, Interannual variability of surface currents in the tropical Pacific during 1987–1993, *J. Geophys. Res., 101,* 3629–3648, 1996.

Halpern, D., Observations of annual and El Niño flow variations at 0°, 110°W and 0°, 95°W during 1980–85, *J. Geophys. Res., 92,* 8197–8212, 1987.

Halpern, D., R. A. Knox, and D. S. Luther, Observations of 20-day period meridional current oscillations in the upper ocean along the Pacific equator, *J. Phys. Oceanogr., 18,* 1514–1534, 1988.

Hayes, S. P., L. J. Mangum, R. T. Barber, A. Huyer, and R. L. Smith, Hydrographic variability west of the Galapagos Islands during the 1982–83 El Niño, *Prog. Oceanogr., 17,* 137–162, 1987.

Jin, F.-F., An equatorial ocean recharge paradigm for ENSO, 1, Conceptual model, *J. Atmos. Sci., 54,* 811–829, 1997.

Johnson, G. C., and M. J. McPhaden, Interior pycnocline flow from the subtropical to the equatorial Pacific Ocean, *J. Phys. Oceanogr., 29,* 3073–3098, 1999.

Johnson, G. C., and D. W. Moore, The Pacific subsurface countercurrents and an inertial model, *J. Phys. Oceanogr., 27,* 2448–2459, 1997.

Kessler, W. S., Observations of long Rossby waves in the northern tropical Pacific, *J. Geophys. Res., 95,* 5183–5217, 1990.

Kessler, W. S., and M. J. McPhaden, The 1991-93 El Niño in the central Pacific, *Deep Sea Res., Part II, 42,* 295–334, 1995.

King, B., and E. Cooper, Comparison of ship's heading determined from an array of GPS antennas with heading from conventional gyrocompass measurements, *Deep Sea Res., Part I, 40,* 2207–2216, 1993.

Kuroda, Y., and M. J. McPhaden, Variability in the western equatorial Pacific Ocean during JAPACS cruises in 1989 and 1990, *J. Geophys. Res., 98,* 4747–4759, 1993.

Mangum, L. J., S. P. Hayes, and J. M. Toole, Eastern Pacific Ocean circulation near the onset of the 1982–1983 El Niño, *J. Geophys. Res., 91,* 8428–8436, 1986.

McPhaden, M. J., Genesis and evolution of the 1997–98 El Niño, *Science, 283,* 950–954, 1999.

McPhaden, M. J., and S. P. Hayes, Variability in the eastern equatorial Pacific during 1986-1988, *J. Geophys. Res., 95,* 13,195–13,208, 1990.

McPhaden, M. J., S. P. Hayes, L. J. Mangum, and J. M. Toole, Variability in the western equatorial Pacific during the 1986–87 El Niño-Southern Oscillation event, *J. Phys. Oceanogr., 20,* 190–208, 1990.

McPhaden, M. J., F. Bahr, Y. Du Penhoat, E. Firing, S. P. Hayes, P. P. Niiler, P. L. Richardson, and J. M. Toole, The response of the western equatorial Pacific Ocean to westerly wind bursts during November 1989 to January 1990, *J. Geophys. Res., 97,* 14,289–14,303, 1992.

McPhaden, M. J., et al., The Tropical Ocean-Global Atmosphere (TOGA) observing system: A decade of progress, *J. Geophys. Res., 103,* 14,169–14,240, 1998.

McTaggart, K. E., and G. C. Johnson, CTD measurements during 1997 and 1998 as part of the Global Ocean-Atmosphere-Land System (GOALS)/Pan American Climate Studies (PACS), *NOAA Data Rep. ERL PMEL-66,* 770 pp., Natl. Oceanic and Atmos. Admin., Silver Spring, Md., 1999.

McTaggart, K. E., M. K. O'Haleck, G. C. Johnson, and L. J. Mangum, CTD measurements during 1995 and 1996 as part of the Global Ocean-Atmosphere-Land System (GOALS)/Pan American Climate Studies (PACS), *NOAA Data Rep. ERL PMEL-62,* 637 pp., Natl. Oceanic and Atmos. Admin., Silver Spring, Md., 1997.

Reverdin, G., C. Frankignoul, E. Kestenare, and M. J. McPhaden, Seasonal variability in the surface currents of the equatorial Pacific, *J. Geophys. Res., 99,* 20,323–20,344, 1994.

Reynolds, R. W., and T. M. Smith, A high-resolution global sea surface temperature climatology, *J. Clim., 8,* 1571–1583, 1995.

Rowe, G. D., E. Firing, and G. C. Johnson, The velocity, transport, and potential vorticity of the Pacific equatorial subsurface countercurrents, *J. Phys. Oceanogr.*, in press, 2000.

Taft, B. A., and W. S. Kessler, Variations of zonal currents in the central tropical Pacific during 1970 to 1987: Sea level and dynamic height measurements, *J. Geophys. Res., 96,* 12,599–12,618, 1991.

Toole, J. M., and M. D. Borges, Observations of horizontal velocities and vertical displacements in the equatorial Pacific Ocean associated with the early stages of the 1982/83 El Niño, *J. Phys. Oceanogr., 14,* 948–959, 1984.

Tsuchiya, M., Upper waters of the intertropical Pacific Ocean, *Johns Hopkins Oceanogr. Stud., 4,* 50 pp., 1968.

Tsuchiya, M., Subsurface countercurrents in the eastern equatorial Pacific Ocean, *J. Mar. Res., 33,* suppl., 145–175, 1975.

Wyrtki, K., and B. Kilonsky, Mean water and current structure during the Hawaii-to-Tahiti shuttle experiment, *J. Phys. Oceanogr., 14,* 242–254, 1984.

Yu, X., and M. J. McPhaden, Seasonal variability in the equatorial Pacific, *J. Phys. Oceanogr., 29,* 925–947, 1999.

Zebiak, S. E., Oceanic heat content and variability and El Niño cycles, *J. Phys. Oceanogr., 19,* 475–486, 1989.

G. C. Johnson, M. J. McPhaden, and K. E. McTaggart, NOAA Pacific Marine Environmental Laboratory, Bldg. 3, 7600 Sand Point Way NE, Seattle, WA 98115. (gjohnson@pmel.noaa.gov)

G. D. Rowe, Department of Oceanography, University of Hawaii, Honolulu, HI 96822.

(Received May 3, 1999; revised August 24, 1999; accepted October 4, 1999.)